



**HAL**  
open science

## Integrated polymer micro-ring resonators for optical sensing applications

Pauline Girault, Nathalie Lorrain, Luiz Poffo, Mohammed Guendouz, Jonathan Lemaitre, Christiane Carré, Michel Gadonna, Dominique Bosc, Guillaume Vignaud

► **To cite this version:**

Pauline Girault, Nathalie Lorrain, Luiz Poffo, Mohammed Guendouz, Jonathan Lemaitre, et al.. Integrated polymer micro-ring resonators for optical sensing applications. *Journal of Applied Physics*, 2015, 117 (10), pp.104504. 10.1063/1.4914308 . hal-01137612

**HAL Id: hal-01137612**

**<https://hal.science/hal-01137612>**

Submitted on 31 Mar 2015

**HAL** is a multi-disciplinary open access archive for the deposit and dissemination of scientific research documents, whether they are published or not. The documents may come from teaching and research institutions in France or abroad, or from public or private research centers.

L'archive ouverte pluridisciplinaire **HAL**, est destinée au dépôt et à la diffusion de documents scientifiques de niveau recherche, publiés ou non, émanant des établissements d'enseignement et de recherche français ou étrangers, des laboratoires publics ou privés.

# Integrated polymer micro-ring resonators for optical sensing applications

Pauline Girault<sup>1</sup>, Nathalie Lorrain<sup>1\*</sup>, Luiz Poffo<sup>1</sup>, Mohammed Guendouz<sup>1</sup>,  
Jonathan Lemaitre<sup>1</sup>, Christiane Carré<sup>1</sup>, Michel Gadonna<sup>1</sup>,  
Dominique Bosc<sup>1</sup> and Guillaume Vignaud<sup>2</sup>

<sup>1</sup>UMR FOTON, CNRS, Université de Rennes 1, Enssat, F22305, Lannion, France

<sup>2</sup>Université Bretagne-Sud, EA 4250, LIMATB, F56100 Lorient, France

\* Corresponding author: nathalie.lorrain@univ-rennes1.fr

## Abstract

Micro-resonators (MR) have become a key element for integrated optical sensors due to their integration capability and their easy fabrication with low cost polymer materials. Nowadays, there is a growing need on MRs as highly sensitive and selective functions especially in the areas of food and health. The context of this work is to implement and study integrated micro-ring resonators devoted to sensing applications. They are fabricated by processing SU8 polymer as core layer and PMATRIFE polymer as lower cladding layer. The refractive index of the polymers and of the waveguide structure as a function of the wavelength are presented. Using these results, a theoretical study of the coupling between ring and straight waveguides has been undertaken in order to define the MR design. Sub-micronic gaps of 0.5  $\mu\text{m}$  to 1  $\mu\text{m}$  between the ring and the straight waveguides have been successfully achieved with UV (i-lines) photolithography. Different superstrates such as air, water and aqueous solutions with glucose at different concentrations have been studied. First results show a good normalized transmission contrast of 0.98, a resonator quality factor around  $1.5 \times 10^4$  corresponding to a coupling ratio of 14.7 % and ring propagation losses around 5 dB/cm. Preliminary sensing experiments have been performed for different concentrations of glucose; a sensitivity of  $115 \pm 8$  nm/RIU at 1550 nm has been obtained with this couple of polymers.

## Introduction

Biological and chemical optical sensors are an active research topic for their many potential applications in medical diagnostics, screening of chemical compounds in drug development, food safety, environment monitoring and security defence.<sup>1,2</sup> Among the existing biological and chemical sensors, micro-resonators (MRs) have been demonstrated to be

extremely sensitive and offer the advantage of significantly minimizing the device size, which greatly reduces the amount of molecules to be detected.<sup>3,4</sup> MRs based on integrated optical waveguides possess promising performances, particularly thanks to their integration capability with electronic devices as well as photonic devices, and to their easy fabrication with mature semiconductor processing technologies.<sup>5-7</sup> Moreover, these sensors allow label-free detection, compatibility with micro-fluidic handling and capability of providing high specificity using surface chemical modifications.<sup>8,9</sup> They can be easily implemented using polymer materials with a low cost of fabrication.<sup>10,11</sup> Most of the MR sensors rely on evanescent wave to detect the presence of molecules whether adsorbed on the sensor surface (surface sensing) or spread in the surrounding medium (homogeneous sensing).<sup>12</sup> The interaction between these molecules and the evanescent waves induces a shift in the specific resonance wavelength  $\Delta\lambda$  due to the refractive index ( $n_c$ ) variation of the upper cladding of the resonator waveguide. In this case, the sensitivity (S) of the sensing optical function is given by  $S = \Delta\lambda/\Delta n_c$  expressed in nm/RIU (Refractive Index Unit).

The context of this work is to improve optical sensor sensitivity based on easily integrated micro-resonator (MR) component. We present a preliminary study on polymer integrated MR with sub-micronic ring waveguide gaps for sensing applications by taking advantage of our previous experiments on filters based on MRs.<sup>13,14</sup> SU8 polymer as core layer and PMATRIFE polymer as lower cladding layer have been chosen due to their refractive index contrast ( $\sim 0.17$  at 1550 nm). First results of such MR using PMATRIFE as lower and upper cladding layers have been recently published.<sup>15</sup> This current work carries out the study of MR structures with the same couple of polymers, but without an upper cladding layer to allow laying of solutions such as glucose aqueous solutions for sensing applications.

After theoretical reminders used in the calculations of MRs characteristics, we present the refractive index study of the polymer waveguide. Micro-ring implementation is then described. A coupling study of the design is presented taking into account different upper cladding mediums. Measurements of extinction responses obtained with MRs with different upper cladding layers are presented and adjusted to theoretical ones in order to determine the group index, coupling and loss parameters. Optical results are discussed taking into account SEM observations and the results obtained in the coupling study. Finally first results of homogeneous sensing experiments using glucose aqueous solution are presented.

## I. Principle

The configuration studied in this work is a single side coupled micro-ring resonator represented in Figure 1. Using a broadband source, wavelengths injected through the first waveguide are coupled into the ring. Those, which are in tune with the incident wave ( $\Sigma\lambda$ ) after a round-trip in the ring, resonate by constructive interferences in the ring. The spectrum observed at the output of the straight waveguide shows extinction for each resonant wavelength.

In the coupling region considered as symmetrical,  $\tau^2$  is the self-coupling ratio in the straight or the ring waveguides whereas  $\kappa^2$  is the cross-coupling ratio as well from the straight waveguide to the ring waveguide at the entrance as from the ring waveguide to the straight waveguide at the exit.

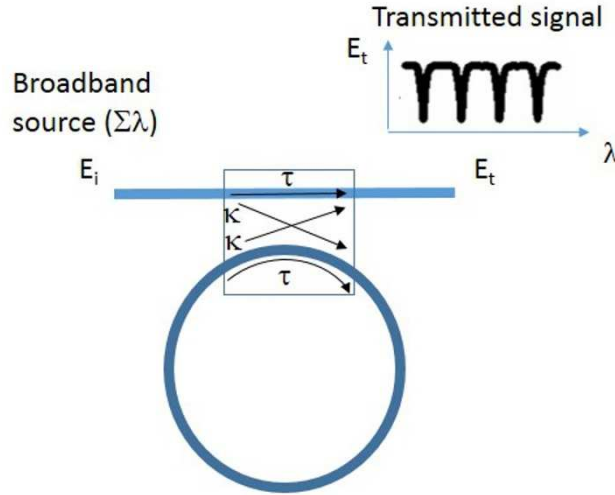


FIG. 1. Single side coupled micro-ring resonator. The field amplitudes are denoted by  $E_i$  (incident) and  $E_t$  (transmitted). Self-coupling ( $\tau$ ) and cross-coupling ( $\kappa$ ) amplitude coefficients are indicated.

In this case of symmetrical and lossless coupling,  $\tau^2$  and  $\kappa^2$  verify  $\tau^2 + \kappa^2 = 1$ , and the normalized transmitted intensity can be expressed<sup>16</sup> by :

$$T(\lambda) = \left| \frac{E_t}{E_i} \right|^2 = \left| \frac{\tau - ae^{j\phi}}{1 - a\tau e^{j\phi}} \right|^2 \quad (1)$$

where: -  $E_i$  and  $E_t$  are respectively the amplitude of the incident and transmitted fields,

-  $\phi = 2\pi R n_{\text{eff}} \beta$  (2) is the single-pass phase shift of the propagated wave in the ring of radius  $R$ , with  $\beta$  the propagation constant and  $n_{\text{eff}}$  the effective index of the ring waveguide.

-  $a = e^{-2\pi R \alpha}$  (3) represents the round trip field attenuation constant and  $\alpha$  the propagation losses per unit length.

The transmission  $T(\lambda)$  has periodic resonances occurring when  $\lambda_{\text{res}} = \frac{2\pi R n_{\text{eff}}}{p}$  (4), corresponding to a single pass phase shift equal to an integer ( $p$ ) times  $2\pi$ :  $\phi = p 2\pi$ .

Two consecutive wavelengths extracted from the ring are separated by a FSR (Free Spectral Range),  $\text{FSR} = \frac{\lambda_{\text{res}}^2}{2\pi R n_g}$  (5), where  $n_g$  is the group index which can be expressed as a function of wavelength and effective index by:

$$n_g(\lambda) = n_{\text{eff}}(\lambda) - \lambda \frac{dn_{\text{eff}}}{d\lambda} \quad (6).$$

$Q = \frac{\lambda_{\text{res}}}{\delta\lambda}$  (7) is the quality factor (with  $\delta\lambda$  the full width at half maximum of the resonance peak)

and the transmission contrast is expressed by the difference ( $T_{\text{max}} - T_{\text{min}}$ ) (8) in which  $T_{\text{max}}$  is the maximum of the transmission and  $T_{\text{min}}$ , the minimum of transmission at the resonant wavelength. FSR,  $Q$  and transmission contrast are the characteristic values of MRs taken into account in this study. They depend, for a given design, on the coupling ratio between the ring and the straight waveguide and on the round trip losses.

## II. Micro-ring implementation

### A. Materials

In this paper, we present the fabrication of micro-ring resonators using Epoxy photoresist SU8 as core material and PMATRIFE (Poly (2,2,2 MethAcrylate of TRIFluoro-Ethyle )) polymer as cladding layer. No upper cladding layer is used unlike in our previous study<sup>15</sup> to implement the structure for sensing applications. SU8 is often used in polymer integrated optics for its optical and chemical properties, as well as its biological compatibilities.<sup>17</sup> To ensure a sufficient light confinement in the waveguide ridge core, PMATRIFE polymer, which offers a relatively low refractive index, has been chosen.

Refractive index evolution of these two polymers as a function of wavelength was investigated by spectroscopic ellipsometry, under ambient conditions (*i.e.* at 25°C and 55% of relative humidity). In each case, a uniform layer of polymer was deposited on a cleaned wafer of silicium by spin-coating at room temperature. Tetrahydrofuran was used as solvent to dissolve PMATRIFE. The solution was spin-cast at rotation speed of 4000 rpm during 10 seconds, to control the thicknesses of the films. After deposition, the samples were further processed by a two-step thermal treatment (10 minutes at 120°C, then 5 hours at 150°C), to evaporate all the solvents and to optimize its mechanical properties. SU8 corresponding to a liquid formulation was used without solvent. The solution was spin-cast first at rotation speed of 500 rpm during 5 seconds and after at 3000 rpm during 20 seconds. Finally, the samples were also processed by a two-step thermal treatment (first 1 minute at 65°C, after the temperature is increased gradually up to 95°C for a total duration of 4 minutes, the sample being at 95°C during 1 minute).

The ellipsometer (Jobin Yvon–Uvisel instrument) was mainly composed of a Xenon source, ranging from long-range ultraviolet to infrared (250-1700 nm), a polarizer, an analyzer and a monochromator handling the dispersion and the selection of the wavelength to a photomultiplier. Each sample was measured at three incident angles 65°, 70° and 75°. Measurements were fitted with a Cauchy layer model, which is composed of a silicon substrate with a 2-nm-thick native SiO<sub>2</sub> layer and a polymer film on top<sup>18</sup>. The fitting parameters were the refractive index of the polymer film, its thickness and the angle of incidence. The obtained thicknesses were  $2.15 \pm 0.10 \mu\text{m}$  for PMATRIFE and  $1.05 \pm 0.05 \mu\text{m}$  for SU8.

On figure 2, the refractive index of SU8 and PMATRIFE materials are plotted as function of wavelength from 1200 nm to 1630 nm for an incident angle of 70°. Refractive index at 1550 nm is then equal to  $1.579 \pm 0.002$  for SU8 polymer and to  $1.411 \pm 0.002$  for PMATRIFE polymer at 25°C. The measurement uncertainties were estimated from the variance of 7 measurements at several locations on three different samples. The values of the refractive index are consistent with the literature; the difference can be explained by the influence of pre-exposure thermal treatments on refractive index, as reported for SU8 by D. Salazar Miranda *et al.*<sup>19</sup>

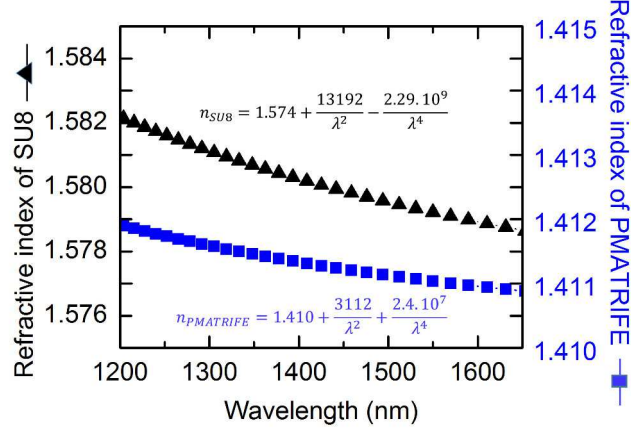


FIG. 2. Refractive index evolution of SU8 and PMATRIFE polymers as a function of the wavelength.

To provide single mode propagation and high confinement, dimensions of SU8 waveguide ridge core are  $1.5 \mu\text{m} \times 1.5 \mu\text{m}$ . The PMATRIFE lower cladding layer thickness is  $7 \mu\text{m}$ . The effective refractive indices of this waveguide for different wavelengths in the range  $[1460 - 1600 \text{ nm}]$  were obtained with the Finite Difference Generic method which is a full vectorial solver of Olympios simulation software. Three upper cladding layers were studied: air, deionized water and glucose aqueous solution ( $100 \text{ g/l}$ ) regarding the sensing applications. The effective index variation as a function of wavelength has been fitted by a linear function over the studied range (Figure 3). Taking into account the refractive index dispersion (equation (6)) mentioned in section I, the group index of the polymer waveguides have been deduced for the three configurations at  $1550 \text{ nm}$ . For air upper cladding layer:  $n_g = 1.657 \pm 0.002 \text{ RIU}$  whereas for deionized water cladding layer,  $n_g = 1.627 \pm 0.002 \text{ RIU}$  and for glucose aqueous solution ( $100 \text{ g/l}$ ),  $n_g = 1.625 \pm 0.002 \text{ RIU}$ .

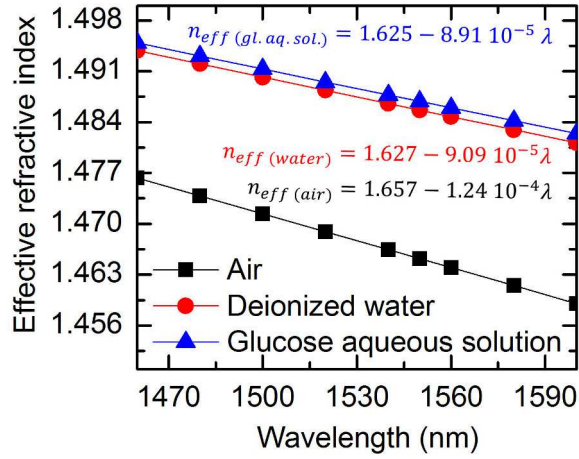


FIG. 3. Effective index evolution of SU8 / PMATRIFE waveguides as function of the wavelength with a SU8 ridge core dimensions of  $1.5 \mu\text{m} \times 1.5 \mu\text{m}$ . Different waveguide upper cladding layers were studied regarding the sensing applications: air, deionized water without and with 100 g/l of glucose.

## B. Design and fabrication

Compared to our previous study of PMATRIFE / SU8 / PMATRIFE MR, we used the structure without PMATRIFE upper cladding layer which has been replaced by air or water superstrates for sensor applications. Nevertheless, we have used the same photolithography mask, the design of which is reminded hereafter. Then we have verified thanks to a coupling study that the gap range is suitable to the SU8 / PMATRIFE MR characteristics values taking into account air and water superstrates.

In order to neglect the bend loss propagation in the ring while keeping in mind the optical integration, a radius of  $120 \mu\text{m}$  has been chosen.<sup>20</sup> Using the equation (5), the calculated FSR of 2 nm will allow a relatively large detection window to be explored. The gap separation between the straight waveguide and the ring is an important parameter which is linked to the coupling ratio. Gaps varying from 0.5 to  $1 \mu\text{m}$  have been studied regarding the theoretical photolithography resolution limit of  $0.4 \mu\text{m}$ .<sup>21</sup>

Such designed waveguides have been realized using photolithography steps.<sup>15</sup> In class 100 clean-room, all the polymer solutions used during the process (Figure 3) were filtered at  $0.2 \mu\text{m}$  before the spin-coating steps. A  $7 \mu\text{m}$ -thick layer of PMATRIFE (500 g/l in THF solvent) was deposited by spin coating on  $200 \mu\text{m}$ -thickness silicon substrate. The deposited layer is exposed to an oxygen plasma RIE (Reactive Ion Etching) to promote the SU8



adherence. A 1.5  $\mu\text{m}$ -thick layer of SU8 is spin-coated and annealed with a temperature ramp up to 95°C. Over the SU8 core, a thin layer of silica ( $\sim 25$  nm) and then another of positive photo-sensitive resin ( $\sim 400$  nm) have been deposited. The thin  $\text{SiO}_2$  layer allowed the protection of SU8 from the next UV exposure step. Then, patterns were produced through a chrome photolithography mask under UV exposure and developed. To obtain the desired waveguides, an oxygen plasma RIE was performed. The top view and the cross section of the obtained waveguides at the end of the process are schematized in Figure 4.

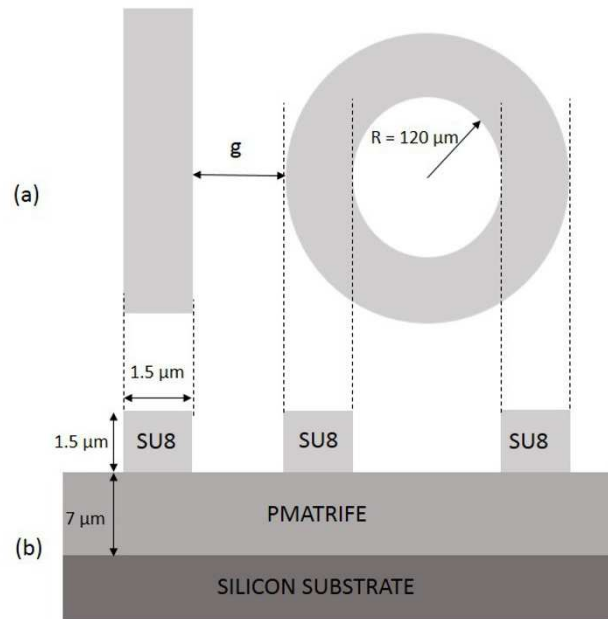


FIG. 4. Schema of a top view (a) and a cross section (b) of the micro-ring resonator.

### C. Coupling study

In order to determine the coupling ratio between the straight and the ring waveguides as function of the gap  $g$  between them, we have used the Marcatili method<sup>22</sup> considering two different upper cladding layers: air and water. All the calculations were performed using Matlab software. Figure 5.a represents the top view of the geometrical coupling area that we have considered and which includes the straight waveguide and half of the ring waveguide. On the cross section view (figure 5.b) are schematized the straight and the ring core waveguides (refractive index  $n_1$ ) surrounded by the lower (refractive index  $n_2$ ) and upper cladding (refractive index  $n_3$ ) layers at the minimal separation gap  $g$ .

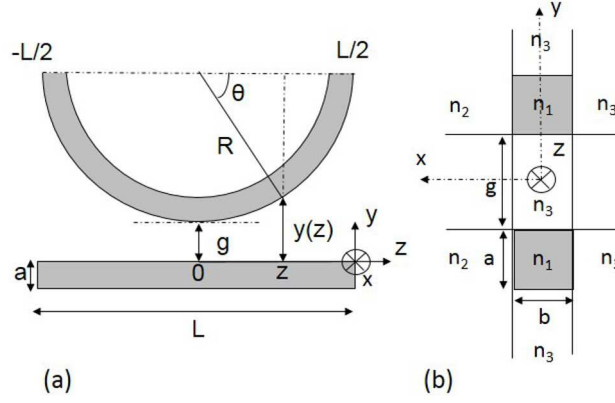


FIG. 5. Schema of the coupling region of micro-ring resonator: (a) top view and (b) cross section view at  $z=0$ .

In this configuration, the distance separation in the  $y$  direction varying along the  $z$  direction can be expressed by the following equation:

$$y(z) = g + R(1 - \cos(\theta)) \quad (9).$$

where  $g$  is the minimal distance between the straight and the ring waveguides,  $R$  the ring radius and  $\theta = \arcsin\left(\frac{z}{R}\right)$  is varying in this configuration from  $-\frac{\pi}{2}$  to  $\frac{\pi}{2}$ .

We note  $C_{TE}(z)$  the coupling coefficient for a  $z$  abscissa given in Marcattili method<sup>22</sup> for the mode TE :

$$|C_{TE}(z)| = 2 \left(\frac{k_x A_3}{\pi}\right)^2 \frac{k_1}{k_z} \frac{\left[1 - \left(\frac{n_3}{n_1}\right)^2\right]^{\frac{1}{2}}}{a} \left[1 - \left(\frac{k_x A_3}{\pi}\right)^2\right]^{\frac{1}{2}} \exp\left\{-\pi \frac{y(z)}{A_3} \left[1 - \left(\frac{k_x A_3}{\pi}\right)^2\right]^{\frac{1}{2}}\right\} \quad (10)$$

where:

- $a$  is the core waveguide width (in the  $y$  transverse direction),
- $k_z$  is the axial propagation constant which depends on the transverse propagation constants  $k_x$  and  $k_y$ , and on the propagation constant  $k_1$  in the free space medium of refractive index  $n_1$ ;

$$k_z = \left(k_1^2 - k_x^2 - k_y^2\right)^{\frac{1}{2}}$$

$$k_x = \frac{\pi}{a} \left( 1 + \frac{2n_3^2 A_3}{\pi n_1^2 a} \right)^{-1}$$

$$k_y = \frac{\pi}{b} \left( 1 + \frac{A_2 + A_3}{\pi b} \right)^{-1}$$

$$k_1 = \frac{2\pi}{\lambda} n_1$$

The transverse propagation constants  $k_x$  and  $k_y$  depend on the refractive indices (figure 5.b.) of the core waveguides ( $n_1$ ), of the lower ( $n_2$ ) and upper cladding layers ( $n_3$ ) and on the coefficients  $A_i$  which are defined for  $i=2,3$  by the expression :

$$A_i = \frac{\pi}{(k_1^2 - k_i^2)^{\frac{1}{2}}}$$

Then to obtain the coupling coefficient  $C_w$  over the whole distance  $L$  of the coupling area (figure 5a), we have to integrate the  $C_{TE}(z)$  function between the abscissa  $-\frac{L}{2}$  to  $\frac{L}{2}$  :

$$C_w = \int_{-\frac{L}{2}}^{\frac{L}{2}} C_{TE}(z) dz \quad (10)$$

Then the coupling ratio  $\kappa^2$  is equal to<sup>23</sup>:

$$\kappa^2 = 1 - (\cos(C_w))^2 \quad (11)$$

$\kappa^2$  is calculated at  $\lambda = 1550$  nm and plotted as a function of the gap  $g$  in figure 6. Within the gap range (0.5  $\mu\text{m}$  to 1  $\mu\text{m}$ ) that can be obtained from a technological point of view, coupling ratio varies from 0 to  $2.45 \pm 0.04$  % for air superstrate and from 0 to  $12.2 \pm 0.3$  % for water superstrate. The uncertainties on the coupling ratio have been estimated taking into consideration the uncertainties on the refractive index of the materials ( section II.A).

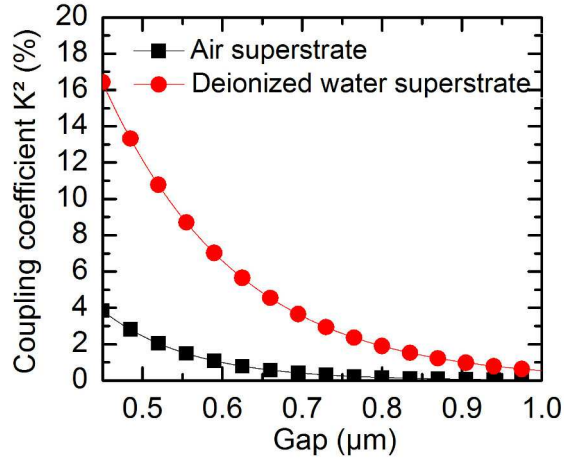


FIG.6. Coupling ratio calculated as function of the gap between the straight and the curved waveguides considering two cases of upper cladding layers: air or deionized water.

For the sensing study, we expect the highest contrast transmission defined by equation (8). The normalized transmission contrast of the MRs as function of the coupling ratio  $\kappa^2$  for 3 different propagation losses is plotted in figure 7 using equation (1). These values of attenuation 1, 3 and 5 dB/cm were chosen in relation to the ring propagation losses of 2.15 dB/cm measured in our previous study<sup>15</sup> and to the material propagation losses of 5 dB/cm in SU8<sup>24</sup>.

In our model used to calculate the normalized transmission, the contrast only depends on the coupling ratio  $\kappa^2$  and the propagation losses. It does not depend on the real effective index that we have calculated previously. Then, the normalized transmission contrast is similar for air and water superstrates.

Figure 7 shows that the maximum of contrast is obtained with a coupling ratio of about 5 % for propagation losses of 1 dB/cm and is about 15 % for losses of 5 dB/cm. According to figure 6, we can approach such coupling values with the gap range of the photolithography mask that we have previously used for PMATRIFE / SU8 / PMATRIFE MR<sup>15</sup>. Thus this gap range of 0.5  $\mu\text{m}$  to 1  $\mu\text{m}$  is suitable to obtain sufficient SU8 / PMATRIFE MR transmission contrast taking into account air and water superstrates.

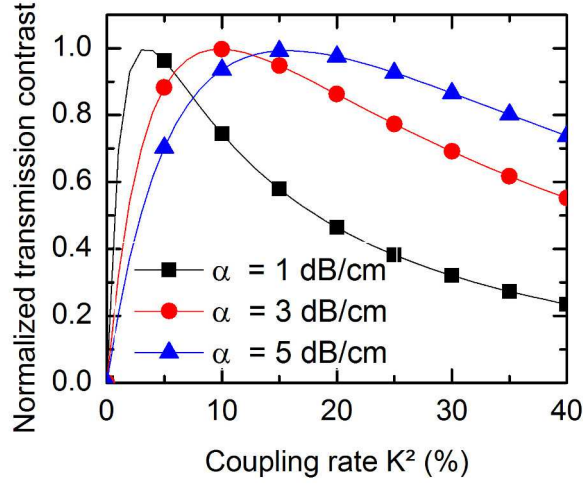


FIG. 7. Normalized transmission contrast plotted in function of the coupling ratio for propagation losses per unit length of 1, 3 or 5 dB/cm at 1550 nm.

### III. Characterizations

#### A. Control of fabrication

Scanning Electronic Microscopy (SEM) observations of MR were performed on the top and on the cross section of the structure to verify its dimensions and assess the quality of the etching edges of the waveguides. A top overview (Figure 8.a) of the micro-ring at low magnification, shows that the ring radius of 120  $\mu\text{m}$  corresponds well to the expected one. Figures 8.b, 8.c and 8.d give a top and a titled views of the coupling region.

The etching edges (Figure 8.d) are quite satisfying at this scale. However, an evaluation of the roughness is difficult to obtain yet we estimated the roughness to be about 50 nm. Moreover, the gap of 0.5  $\mu\text{m}$  has been successfully made (Figure 8.c). Figure 8.e shows a cross section view of the straight ridge waveguide with the suitable dimensions.

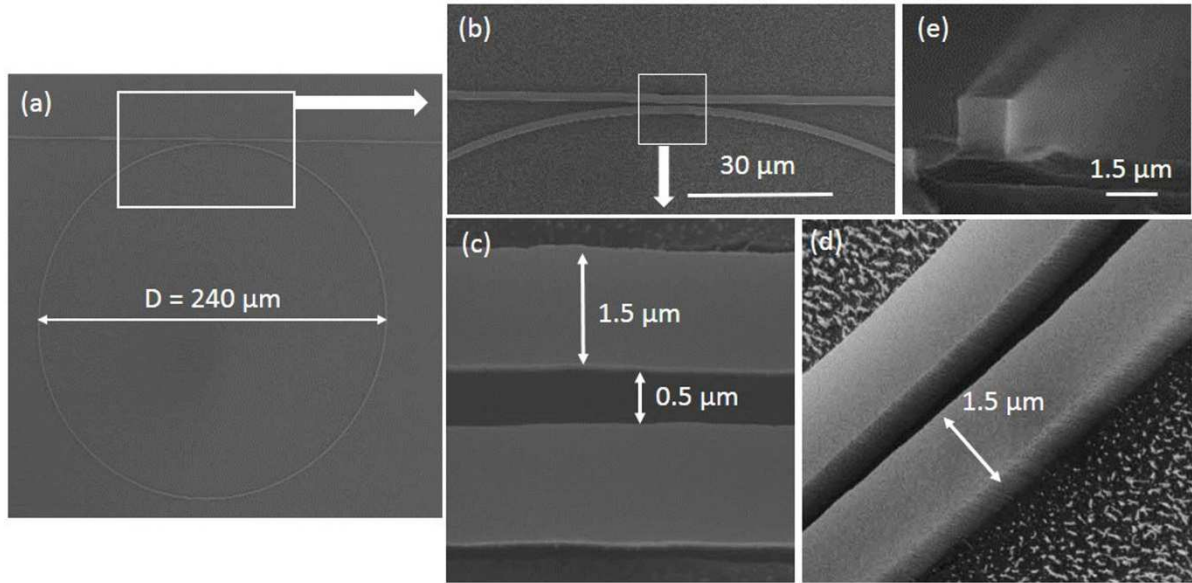


FIG. 8. SEM images of the Air/SU8/PMATRIFE MR. (a) Top overview, (b) and (c) top view of the coupling region. (d) Tilted view of the etched waveguides in the coupling region. (e) Cross section view of the straight ridge waveguide.

## B. Extinction responses

In order to characterize the microresonators, we have measured their spectral responses. A tunable laser (Agilent 8164A with 81680A tunable source) was injected in the input waveguide using a lensed single mode fiber (mode radius of  $2.2 \mu\text{m}$ ). At the output, another lensed single mode fiber is used to couple the output of the waveguide to a power meter or a spectrum analyzer (figure 9).

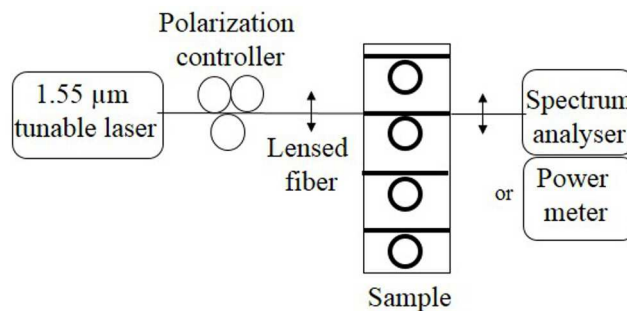


FIG. 9. Overview of the optical MR characterization system.

For sensing applications, it is suitable to have one selected polarization to optimize their characteristic values, such as  $Q$  and transmission contrast, and to make the analysis of the MR

responses easier. Therefore, a polarization controller is inserted between the laser and the input of the lensed fiber.

The measurements of transmission were done on the through port in the wavelength range of 1550-1560 nm with a step of 2.5 pm. The calculated transmission were adjusted to experimental ones using equation (1) defined in section I. The adjustment of resonances shape was performed by modifying the coupling ratio and the propagation losses in the ring whereas the FSR was adjusted with the index group parameter. Figure 10 reports the experimental and the theoretical adjusted spectral responses for the gap of 0.5  $\mu\text{m}$  and for 2 cases of superstrates: (a) air and (b) deionized water. The experimental spectral response of air superstrate was taken after the complete evaporation of water in order to maintain the polarization established in the case of water superstrate, keeping in mind the sensing application.

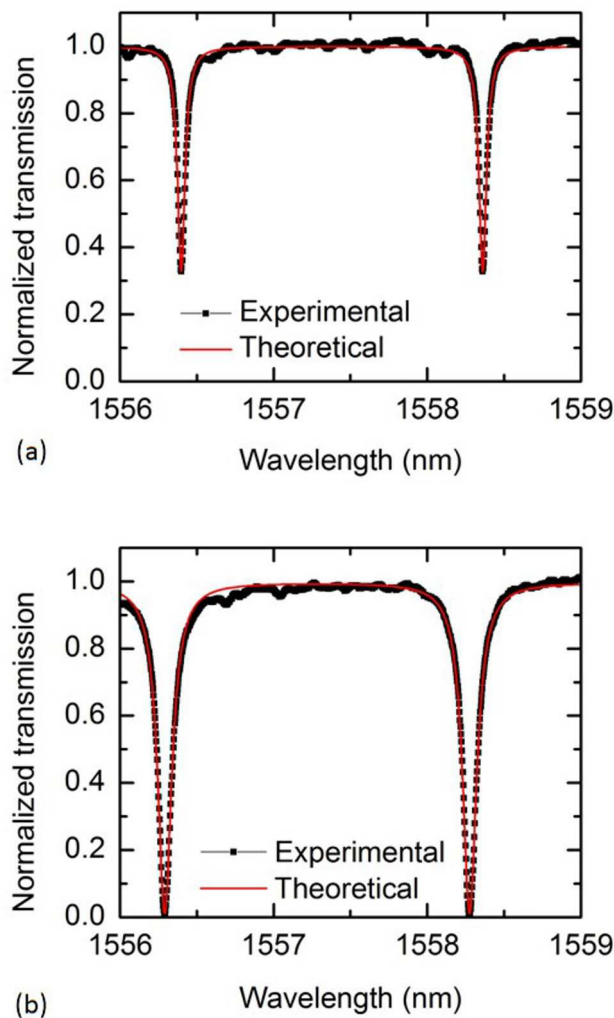


FIG. 10. Experimental and calculated transmission spectra for one polarization light and for the gap of 0.5  $\mu\text{m}$ : (a) for Air/SU8/PMATRIFE and (b) for deionized water /SU8/PMATRIFE micro-rings.

Adjustment parameters with their uncertainties are given in Table I. The expected values for coupling ratio and group index, already reported respectively in figure 6 and figure 3, are also indicated.

TABLE I. Adjustment parameters: coupling ratio, propagation losses in the ring and group index and calculated ones.

WAVEGUIDE	Air/SU8/PMATRIFE		Aqueous solution/SU8/PMATRIFE	
	From adjustment	Calculated	From adjustment	Calculated
Coupling rate (%)	$3.95 \pm 0.05$	$2.45 \pm 0.04$	$14.7 \pm 0.2$	$12.2 \pm 0.3$
Propagation losses (dB/cm)	$4.23 \pm 0.08$	-	$5.55 \pm 0.05$	-
Group index	$1,628825 \pm 10^{-6}$	$1.657 \pm 0.002$	$1,610250 \pm 10^{-6}$	$1.627 \pm 0.002$

The coupling ratio obtained from the Marcatili method is in the two cases lower than the ones obtained from the adjustment of experimental data. The Marcatili method only matches for low refractive index contrasts between the core and the cladding layers. The index contrast of the couple of polymer (SU8/PMATRIFE) is 0.17, value which might be too high to use the Marcatilli method. The limitation of this method for our refractive index contrast values could explain the difference between the coupling ratio obtained by adjustment of the experimental data and the calculated ones. Another reason which could explain this difference could be technological imperfections at nanometer scale that would favor the coupling. From a technological point of view, according to SEM observations, the gap of  $0.5 \mu\text{m}$  is reached with an estimated accuracy of  $0.05 \mu\text{m}$ . If we take into consideration these accuracies on figure 6, the uncertainties of coupling ratio reach nearly 1.5%. This quite high value could thus also explain the difference between the calculated and adjusted coupling ratio.

Estimation of material propagation losses in the ring have been deduced thanks to a fitting of spectral MR response with equation (1).

Material propagation losses around 4 - 5 dB/cm have been obtained for the two studied upper superstrates (air or deionized water). This value is in the same order as other losses



obtained in micro-ring resonators using SU8 for core layer but OG-125 ( $n = 1.456$ ) for lower and upper cladding.<sup>24</sup> If we take this propagation loss value in figure 7, we can observe that the maximum of contrast is obtained for a coupling ratio of 15 %, value which is experimentally reached for deionized water upper cladding. For air upper cladding, taking into consideration the same propagation losses, a contrast of around 0.7 is expected and corresponds to the measured one. On the contrary, the presence of deionized water in the ring rather than air, induces a decrease of the Q factor ( $2.7 \cdot 10^4$  in air against  $1.5 \cdot 10^4$  in deionized water) due to the increase of the coupling ratio. In this case, the contrast nearly reaches the maximum: the measured value is 0.98. For this gap and for the water superstrate case, the coupling is then optimal. We observe an opposite behaviour for group index. The group index obtained from adjustment is lower than the calculated one. The experimental group index is deduced from the equation (5) with FSR and  $\lambda_{\text{res}}$  taken from experimental data and with the ring radius R equal to the expected one (120  $\mu\text{m}$ ). The calculated group index just takes into account the wavelength dispersion. First, it is determined from the experimental material refractive indexes and then from simulation by the finite difference method at several wavelengths. However, the curvature of the ring may also affect the group index, which has not been taken into account.

Concerning the resonant wavelength, the presence of deionized water on the ring rather than air, induced a shift of resonant wavelengths. It can be estimated using the effective index of the waveguide that we have determined (see figure 3). For air upper cladding, the resonant wavelength is 1556.4 nm corresponding to an order p of 700, according to equation (4), with an effective index of 1.464. For deionized water upper cladding, because of the effective index increase, and for the same integer order  $p = 700$ , the resonant wavelength is about 1600.6 nm. The red shift of resonant wavelength induced by the increase of effective index approaches 44 nm which corresponds to nearly 22 times the value of FSR. Consequently, we did not estimate any sensitivity from these measurements.

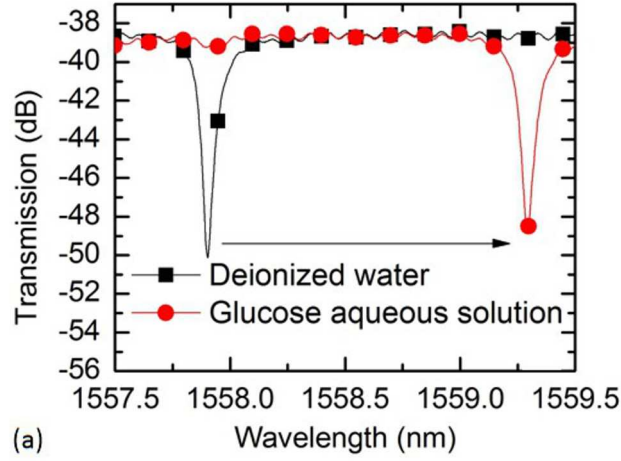
#### **IV. Sensing experiment**

Our interest in this work was to use the MR structure as an optical transducer for sensing applications. For this objective and in order to evaluate the sensitivity of the structure by homogeneous sensing, glucose aqueous solutions were used with different concentrations. The solutions were introduced into the MR structure using a micro-syringe and were kept at the ambient temperature of the experimental room. The studied range of glucose concentration

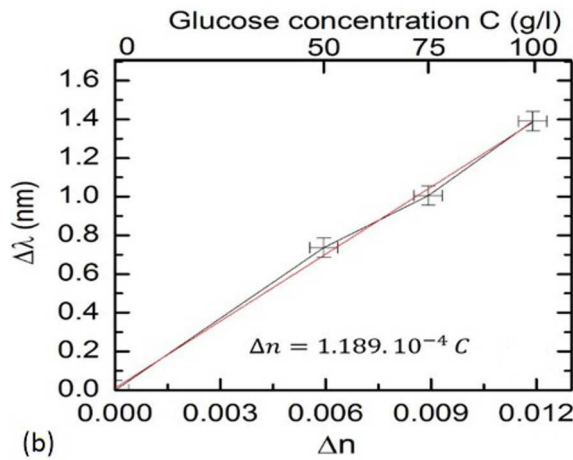
varied from 0 to 100 g/l with an accuracy of 2.5 g/l. This concentration range was chosen to prevent a shift of the resonant wavelength higher than the FSR.

The experimental transmission spectra obtained with deionized water superstrate and with a glucose aqueous solution using a concentration of 100 g/l, are reported in Figure 11.a. In this condition, the increase of the refractive index of deionized water due to the presence of solubilized glucose was 0.012, according to Ciminelli *et al.*<sup>25</sup>. Such a refractive index variation provided a resonant wavelength red-shift of 1.39 nm at around 1558 nm (figure 11.a). In order to estimate the uncertainty on the red-shift, we performed the measurements 3 times by removing the sample from the optical bench. The error on the red shift has been estimated to 0.05 nm. The sensitivity of the MR was, in this case,  $116 \pm 8$  nm /RIU (Refractive Index Unit) corresponding to the wavelength shift variation per upper cladding refractive index variation. In the uncertainty of 8 nm/RIU, both the uncertainties on the red shift and on the glucose concentration have been taken into consideration. We observed a decrease in the contrast of nearly 1 – 2 dB for each studied glucose concentration. The small increase of upper cladding refractive index may induce, for the same gap between the ring and the straight waveguide, a slightly higher coupling ratio. For aqueous solution, the optimal coupling ratio was reached for the gap of 0.5  $\mu$ m. Therefore, by increasing the upper cladding refractive index, the increase of coupling ratio would provide a decrease in the contrast according to Figure 6.

In Figure 11.b, the measured red shifts obtained for glucose concentration of 50, 75 and 100 g/l are plotted as function of the refractive index variation of the aqueous solution with dissolved glucose (Figure 11.b). The sensitivity of our SU8/PMATRIFE MR taking into consideration the different glucose aqueous solutions as upper cladding is around  $115 \pm 8$  nm /RIU. Such sensitivity values are reported in literature for silicon on insulator (SOI) MR<sup>25</sup> and higher sensitivity (300 nm/RIU)<sup>6</sup> was obtained with silicon slot-waveguides-based ring resonator on insulator.



(a)



(b)

FIG. 11. (a) Experimental transmission spectra for one polarization light for deionized water/SU8/PMATRIFE and glucose aqueous solution (100 g/l)/SU8/PMATRIFE micro rings. Wavelength shift ( $\Delta\lambda$ ) of the resonance associated with the change of refractive index ( $\Delta n$ ) of the upper cladding layer. (b) Wavelength shift ( $\Delta\lambda$ ) of the resonance plotted as a function of glucose concentration dissolved in water and as a function of the refractive index change ( $\Delta n$ ) of the upper cladding layer.

## Conclusion

This study aimed to implement integrated polymer MRs for sensing applications using SU8 as core material and PMATRIFE as lower confinement material. Different superstrates such as air, deionized water and glucose aqueous solution were studied. With the aim of determining the index group of the structures, parameter necessary for the simulation study, refractive index of the different polymers, used in the fabrication of MRs, are given as a function of wavelength. To optimize the design of the MRs, a coupling study was performed to link gap and

characteristics values of MRs. These preliminary studies allowed us to implement successfully MRs with sub-micronic gaps varying from 0.5 to 1  $\mu\text{m}$ . The best result is obtained for water superstrate. Normalized transmission contrast of 0.98 with a quality factor of nearly  $1.5 \times 10^4$  was achieved for a gap of 0.5  $\mu\text{m}$  corresponding to a coupling ratio of 14.7 % and ring propagation losses of 5.5 dB/cm according to the theoretical MR responses. The sensing application is tested with different glucose concentrations in water. We have measured a sensitivity of the SU8/PMATRIFE MRs of  $115 \pm 8 \text{ nm/RIU}$  using a couple of polymers which technology is mastered in our lab. Our current work is to increase further the sensitivity by using other core and cladding materials with larger flexibility of their refractive index.

### Acknowledgments

This work is supported by the PONANT project, funded by *Lannion Trégor Communauté, Conseil Général des Côtes d'Armor, Région Bretagne, Feder* and *the French Research Ministry*.

### References

- [1] X. Fan, I. M. White, S. I. Shopova, H. Zhu, J.D. Suter, Y. Sun, *Analytica Chimica Acta* **620**, 8, (2008).
- [2] Y. Sun and X. Fan, *Optics expressed* **16**, 10254, (2008).
- [3] A. Chiasera, Y. Dumeige, P. Féron, M. Ferrari, Y. Jestin, G. Nunzi Conti, S. Pelli, S. Soria, G. C. Righini, *Laser & Photonics Reviews* **4**, 457, (2010).
- [4] G.C. Righini, Y. Dumeige, P. Féron, M. Ferrari, G. Nunzi Conti, D. Ristic, S. Soria. *Rivista del Nuovo Cimento* **34**, 435, (2011).
- [5] D. Duval and L. M. Lechuga, *IEEE Photonics journal* **5**, 1, (2013).
- [6] T. Claes, J. G. Molera, K. De Vos, E. Scharcht, R. Baets, P. Bienstman, *IEEE Photonics journal* **1**, 197, (2009).
- [7] A. Ramachandran, S. Wang, J. Clarke, S. J. Ja, D. Goas, L. Wald, E.M. Flood, E. Knobbe, J.V. Hryniewicz, S.T. Chu, D. Gill, W. Chen, O. King, B.E. Little, *Biosensors and Bioelectronics* **23**, 939, (2008).
- [8] K. De Vos, J. Girones, S. Popelka, E. Schacht, R. Baets, P. Bienstman, *Biosensors and Bioelectronics* **24**, 2528, (2009).
- [9] W. Bogaerts, P. De Heyn, T. Van Vaerenberg, K. De Vos, S. Kumar Selvaraja, T. Claes, P. Dumon, P. Bienstman, D. Van Thourhout and R. Baets, *Laser Photonics Rev.* **6**, 47, (2012).
- [10] M. W. Royal, N. M. Jokerst, R. B. Fair, *IEEE Photonics journal* **4**, 2126, (2012).
- [11] R. Landgraf, A. Finn, R. Kirchner, T. Haugwitz, F. Deicke, W.J. Fischer, S. Arndt,

Tagungsband, 259, (2012).

- [12] C.Y. Chao, W. Fung, L.J. Guo, IEEE journal of selected topics in quantum electronics **12**, 134 (2006).
- [13] A. Maalouf, M. Gadonna, D. Bosc, I. Hardy, Optics Communications **285**, 4088 (2012).
- [14] A. Maalouf, C. Bastianelli, F. Mahé, A. Belmiloudi, M. Gadonna, D. Bosc, Photonics Europe 2012, Silicon Photonics and Photonic Integrated Circuits conference, Brussels, SPIE **8431**,75 (2012).
- [15] P. Girault, J. Lemaitre, M. Guendouz, N. Lorrain, L. Poffo, M. Gadonna, D. Bosc, SPIE Proceedings, Optical Sensing and Detection III **9141**, 76, (2014).
- [16] A. Yariv, Electronics Letters **36**, 321 (2000).
- [17] A. P. Gadre, A. J. Nijdam, J. A. Garra, A. H. Monica., M. C. Cheng, C. Luo, Y. N. Srivastava, T. W. Schneider, T. J. Long, R. C. White, M. Paranjape, J. F. Currie, Sensors and Actuators A **114**, 478, (2004).
- [18] A. El Ouakili, G. Vignaud, E. Balnois, J. F. Bardeau, Y. Grohens, Thin Solid Films, **519** (6), 2031, (2011).
- [19] D. Salazar-Miranda, F.F. Castillon, J.J. Sanchez-Sanchez, J.L. Angel-Valenzuela, H. Marquez, Revista Mexicana de Ingeniera Quimica **9**, 85, (2010).
- [20] A. Maalouf, D. Bosc, P. Grosso, M. Gadonna, M. Thual, F. Henrio and S. Haesaert, Proc. SPIE 6996, Silicon Photonics and Photonic Integrated Circuits, 69991S, (2008).
- [21] A. Maalouf, M. Gadonna, D. Bosc, Journal of Physics D: Applied Physics **42**, 015106, (2009).
- [22] E.A.J. Marcatili, Tech. J. **48**, 2071, (1969).
- [23] K. Okamoto, Fundamentals of optical waveguides, 2<sup>nd</sup> edition, Academic Press, (2006) p.197-198.
- [24] J. K. S. Poon, Y. Huang, G. T. Paloczi, A. Yariv, IEEE Photonics technology letters **16**, 2496, (2004).
- [25] C. Ciminelli, F. Dell'Olio, D. Conteduca, C.M. Campanella, M.N. Armenise, Optics & laser technology **59**, 60, (2014).